PCCP

Accepted Manuscript

ROYAL SOCIETY OF CHEMISTRY

www.rsc.org/pccp

Cite this: DOI: 10.1039/c0xx00000x

www.rsc.org/xxxxxx

ARTICLE TYPE

Novel Flexible Belt-shaped Coaxial Microcables with Tunable Multicolor Luminescence, Electrical Conduction and Magnetism

Hong Shao, Qianli Ma, Xiangting Dong*, Wensheng Yu, Ming Yang, Ying Yang, Jinxian Wang, Guixia Liu

Received (in XXX, XXX) Xth XXXXXXXXX 20XX, Accepted Xth XXXXXXXXX 20XX
DOI: 10.1039/b000000x

A novel type of flexible [Fe_3O_4/PANI/PMMA]@{[$Eu(BA)_3$phen+$Tb(BA)_3$phen]/PMMA} (PMMA= polymethyl methacrylate, BA= benzoic acid, phen= phenanthroline, polyaniline= PANI) belt-shaped coaxial microcables possessing electrical conductivity, magnetism and color-tunable photoluminescence has been successfully fabricated by electrospinning technology using a specially designed coaxial spinneret. Every strip of belt-shaped coaxial microcable is assembled with a Fe_3O_4/PANI/PMMA electrically conductive-magnetic bifunctional core and a [$Eu(BA)_3$phen+$Tb(BA)_3$phen]/PMMA insulative and photoluminescence-tunable shell. The conductivity of the core of belt-shaped coaxial microcables reaches up to the order of 10^{-2} $S \cdot cm^{-1}$ and all belt-shaped coaxial microcables are insulated from each other. The tuning of emission color is possible by changing the Eu^{3+}/Tb^{3+} molar ratio of the belt-shaped coaxial microcables. The electrical conductivity, magnetic and photoluminescent properties of belt-shaped coaxial microcables can be tuned by adjusting the contents of PANI, Fe_3O_4 nanoparticles (NPs) and rare earth complexes. More importantly, the proposed design idea and construction technique are of universality for preparing other multifunctional one-dimensional micromaterials.

1 Introduction

Recently, there has been growing research interest in the design and fabrication of novel multifunctional materials, since novel multifunctional nano/microcomposites provide the possibility for multifunctional properties and enhanced functionality in contrast to their more-limited single functional nano/micromaterials.[1-4] For instance, nano/microcomposites with both fluorescent and magnetic properties can be used in a wide range of applications in biological systems, such as controllable drug release[5], bioimaging[6, 7], diagnostic and therapeutics[7]. Electrical conduction-magnetism functionalized micro/nanostructures are of special interest due to their potential applications in areas such as electromagnetic interference shielding[8], microwave absorption[9] and biomedicine[10].

The Fe_3O_4 nanoparticles (NPs) are the most widely studied magnetic nanoparticles not only for the fundamental magnetic properties, but also for biomedical applications[11]. It is well known that polyaniline (PANI), as one of the most conducting polymers, has been extensively explored and used in many areas such as electrochromic devices, secondary batteries, catalysis and biosensors owing to its good electrical conductivity, reversible redox property and good environmental stability.[12-14]

At present, some preparations of one-dimensional luminescent-electrical-magnetic multifunctional materials have been reported. Magnetic-fluorescent bifunctional composite nanofibers[15, 16], composite nanoribbons[17], photoluminescence-electrical conduction bifunctional composite nanofibers[18], photoluminescence-electricity-magnetism trifunctional composite nanofibers[19], composite nanobelts[20] as well as electricity-magnetism and color-tunable microbelts[21] have been prepared *via* electrospinning. On the basis of these studies, the nano/microcomposites suffered heavy losses in fluorescent intensity when Fe_3O_4 NPs and PANI were blended with the luminescent compounds. Therefore, luminescent compounds should be effectively isolated from Fe_3O_4 NPs and PANI to avoid direct contact.

RE luminescent materials emitting multiple colors have aroused extensive attention because of their important role in the field of light display systems, lasers and optoelectronic devices[22, 23]. Rare earth ions generally have plenty of well-shielded 4f states that can emit fluorescence covering different wavelength from ultraviolet to infrared. For example, Tb^{3+} can emit green rays and the red-emitting components can be achieved by the emission of Eu^{3+}. Recently, Liu, *et al.*[24] investigated the luminescence properties of Y_2O_3: RE^{3+} (RE= Eu, Tb) and Y_2O_3: Eu^{3+}, Tb^{3+} phosphors by changing the concentration of Tb^{3+} and Eu^{3+}. From the excitation and emission spectra of codoping samples, there exist two kinds of samples characteristic of red emission and green emission due to Eu^{3+} and Tb^{3+} ions in Y_2O_3 host, respectively. Zeng[25] synthesized $Gd_2(WO_4)_3$ structures which were good host matrixes and showed strong multi-color photoluminescence (PL) emissions. Tunable emissions have been achieved in the Eu^{3+}/Tb^{3+} co-doped samples, owing to the strong absorption of tungstate ions. Among various luminescent

materials, rare earth complexes doped inorganic/organic hybrids have good thermal and mechanical stabilities and processing property. Furthermore, they have excellent luminescent property on account of the antenna effect of ligands and the f-f electron transition of RE^{3+} ions.

With the rapid development of nano/micro-technology in recent years, fabrication and application of microcables are becoming more and more crucial. Up to now, some types of microcables have been synthesized. The researchers have adopted carbon fibers or tubes, metal materials, conductive polymers and other conductive materials as the inner conductor of microcables.[26-30] The shell must have good insulation property and, sometimes, have other functions. Belt-shaped one-dimensional (1D) materials have attracted increasing interest from scientists owing to their anisotropy, large width-thickness ratio, unique optical, electrical, and magnetic properties. Moreover, belt-shaped cables have better anti-entangling performance and smaller winding volume, and they have higher electrical conduction than the traditional fibers with the same components. Inspired by the structure of microcable, in this work, we designed and fabricated novel belt-shaped coaxial microcable composed of a Fe_3O_4 NPs/PANI/polymethyl methacrylate (PMMA) core and a RE (RE= Eu, Tb) complexes/PMMA shell. By constructing such kind of structure, luminescent compounds can be effectively isolated from Fe_3O_4 NPs and PANI to avoid direct contact. The new type of belt-shaped coaxial microcable composed of a conductive core and an insulative shell is ideally suited to be applied in high density electrical connections in narrow spaces, such as in mobile phones, subminiature integrated circuits, microchips and nano/micro-machines[31, 32]. Furthermore, magnetic and photoluminescent properties are introduced into the belt-shaped coaxial microcable to realize multifunctionality. Herein, magnetism endows the belt-shaped coaxial microcable controllability under external magnetic field, and photoluminescence gives it visibility. These characteristics allow the belt-shaped coaxial microcables to be widely used in biological systems, such as bioimaging, diagnostic, targeting and therapeutics[33, 34]. The multifunctional belt-shaped coaxial microcables can be applied in the field of electromagnetic interference shielding [35, 36] and full-color display[21]. The structure, conductivity, fluorescence, and magnetism of the belt-shaped coaxial conductive microcables were studied, and some new results were obtained.

2 Experimental section

Chemicals

Eu_2O_3 (99.99 %), Tb_4O_7 (99.99 %), benzoic acid (BA), 1,10-phenanthroline (phen), $FeCl_3{\cdot}6H_2O$, $FeSO_4{\cdot}7H_2O$, NH_4NO_3, polyethylene glycol (PEG, Mr ≈ 20,000), methylmethacrylate (MMA), benzoylperoxide (BPO), ammonia, $CHCl_3$ and *N,N*-dimethylformamide (DMF) were bought from Tianjin Tiantai Fine Chemical Co., Ltd. Anhydrous ethanol, aniline (ANI), (IS)-(+)-Camphor-10 sulfonic acid (CSA) and Oleic acid (OA) were purchased from Sinopharm Chemical Reagent Co., Ltd. Ammonium persulfate (APS) was bought from Guangdong Xilong Chemical Co., Ltd. Nitric acid (HNO_3, AR) was purchased from Beijing Chemical Works. MMA was purified by reduced pressure distillation to remove polymerization inhibitor. All the other reagents were of analytical grade and directly used as received without further purification.

Synthesis of of rare earth complexes

$Tb(BA)_3$phen complexes were synthesized according to the traditional method as described in the literature[37]. 0.9346 g of Tb_4O_7 was dissolved in 20 mL of concentrated nitric acid at 60 °C. Then $Tb(NO_3)_3{\cdot}6H_2O$ powders were acquired by evaporation of excess nitric acid and water by heating. $Tb(NO_3)_3$ ethanol solution was prepared by adding 20 mL of anhydrous ethanol into the above $Tb(NO_3)_3{\cdot}6H_2O$. 1.8320 g BA and 0.9910 g of phen were dissolved in 200 mL of ethanol. $Tb(NO_3)_3$ ethanol solution was then added into the mixture solution of BA and phen under magnetic stirring for 3 h at 60 °C. The precipitates were collected by filtration and dried for 12 h at 60 °C. The synthetic method of $Eu(BA)_3$phen complex was similar to the above method, except that the using dosages of Eu_2O_3, BA and phen were 0.1760 g, 0.3664 g and 0.1982 g, respectively.

Preparation of PMMA

PMMA used in this study was prepared by oxidative polymerization of MMA.[38] Refined MMA (100 mL) and BPO (0.1000 g) were mixed in a 250-mL three-necked flask with a backflow device and stirred vigorously at 90-95 °C. When the viscosity of the solution reached a certain value just like that of glycerol, the heating was stopped and it was left to naturally cool down to room temperature. The obtained gelatinous solution was then loaded into test tubes, and the influx height was 5-7 cm. After that, the tubes were put in an electric vacuum oven for 48 h at 50 °C, and the gelatinous solution was then solidified. Finally, the temperature in the oven was raised to 110 °C for 2 h to terminate the reaction.

Preparation of oleic acid modified Fe_3O_4

Monodispersed Fe_3O_4 NPs with a narrow size distribution were prepared using the chemical co-precipitation method[39]. In order to prevent the particles from aggregating, PEG was used as the protective agent. In a typical procedure, 5.4060 g of $FeCl_3{\cdot}6H_2O$, 2.7800 g of $FeSO_4{\cdot}7H_2O$, 4.0400 g of NH_4NO_3 and 1.9000 g of PEG were added into 100 mL of deionized water to form a uniform solution under the protection of argon atmosphere with vigorous stirring at 50 °C. After the mixture had been bubbled with argon for 30 min, 0.1 mol/L of $NH_3{\cdot}H_2O$ was added dropwise into the mixture until the pH value was above 11. Black precipitates were formed quickly, and the resultant solution was kept stirring for another 30 min under argon at 50 °C. Subsequently, the product was separated by using a magnet and washed with distilled water three times, and then dried in an electric vacuum oven at 60 °C for 12 h.

To improve the monodispersity, stability and solubility of Fe_3O_4 NPs in the spinning solution, the as-prepared Fe_3O_4 NPs were then coated with oleic acid (OA) as below: 2.0000 g of the as-prepared Fe_3O_4 NPs were ultrasonically dispersed in 100 mL of deionized water for 20 min. The suspension was heated to 80 °C under argon atmosphere with vigorous mechanical stirring for 30 min and then 1 mL of OA was dropwise added. Reaction was stopped after heating and stirring the mixture for 40 min. The precipitates were collected from the solution by magnetic

separation, washed with ethyl alcohol for three times, and then dried in an electric vacuum oven at 60 °C for 6 h.

Preparations of spinning solutions for fabricating belt-shaped coaxial microcables

Two different kinds of spinning solutions were prepared to fabricate belt-shaped coaxial microcables. The spinning solution for preparing the shell of belt-shaped coaxial microcables consisted of certain amounts of $Eu(BA)_3phen$, $Tb(BA)_3phen$ (Specific amounts are indicated in Table 1), 0.5 g of PMMA, 9 g of $CHCl_3$ and 0.9 g of DMF (denoted as spinning solution I).

For the preparation of the core spinning solution, oleic acid modified Fe_3O_4 was dissolved in the mixed solution of 0.3 g of DMF and 6 g of $CHCl_3$, then dispersed ultrasonically for 15 min, and then PMMA, CSA and ANI were slowly added into the above solution with magnetic stirring for 48 h at room temperature (defined as solution A). Meanwhile, APS was used as an oxidant and dispersed into a mixed solution of 0.6 g of DMF and 3 g of $CHCl_3$ with magnetic stirring for at least 2 h at room temperature (defined as solution B). Then solutions A and B were both cooled down to 0 °C in an ice-bath. Subsequently, solution B was added dropwise into solution A under magnetic stirring. The final mixture was allowed to react at 0 °C for 24 h to produce PANI by the polymerization of ANI[40, 41]. The final mixture was denoted as spinning solution II, which was used to fabricate the core of $[Fe_3O_4/PANI/PMMA]$@{$[Eu(BA)_3phen+Tb(BA)_3phen]$/PMMA} belt-shaped coaxial microcables. The dosages of these materials were summarized in Table 2.

Table 1 Compositions of the spinning solution I

Spinning solution I	$Eu(BA)_3phen$: $Tb(BA)_3phen$ (mass ratio)	$Eu(BA)_3$ phen/g	$Tb(BA)_3$ phen/g	PMMA/ g
S_{a1}	10:0	0.075	0	0.5
S_{a2}	9:1	0.0675	0.0075	0.5
S_{a3}	7:3	0.0525	0.0225	0.5
S_{a4}	5:5	0.0375	0.0375	0.5
S_{a5}	3:7	0.0225	0.0525	0.5
S_{a6}	1:9	0.0075	0.0675	0.5
S_{a7}	0:10	0	0.075	0.5

Table 2 Compositions of the spinning solution II

Spinning solution II	Composition				
	ANI /g	CSA /g	APS /g	PMMA /g	Fe_3O_4 /g
S_{b1}	0.15	0.2809	0.3676	0.5	0.5
S_{b2}	0.15	0.2809	0.3676	0.5	1.5
S_{b3}	0.15	0.2809	0.3676	0.5	2.5
S_{b4}	0.25	0.4682	0.6126	0.5	1.5
S_{b5}	0.35	0.6554	0.8578	0.5	1.5

Fabrication of tunable multicolor-electricity-magnetism trifunctional belt-shaped coaxial microcables

A homemade coaxial electrospinneret was used in this study. The equipment for the electrospinning process is presented in Figure 1. Spinning solution I was loaded into the outer plastic syringe while spinning solution II was loaded into the inner plastic syringe. A piece of flat iron net was used as a collector and put about 10 cm away from the nozzle tip. The positive terminal of a direct current DC high voltage power supply was connected to the carbon electrode which was immersed into the spinning solution II, and the negative terminal was connected to the iron net. Positive DC voltage of 6 kV was applied between the nozzle and the collector to generate belt-shaped coaxial microcables under the ambient temperature of 20-25 °C, and the relative humidity of 45-50 %.

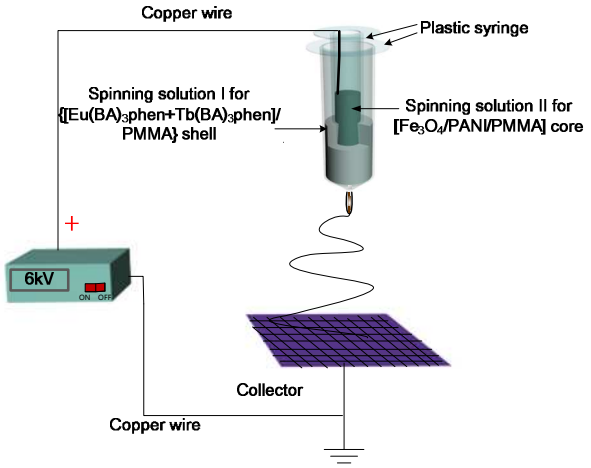

Figure 1 Schematic diagram of the specially designed coaxial spinneret and electrospinning setup.

Fabrication of Fe_3O_4/$[Eu(BA)_3phen+Tb(BA)_3phen]$/PANI/PMMA composite microbelts

Meanwhile, Fe_3O_4/$[Eu(BA)_3phen+Tb(BA)_3phen]$/PANI/PMMA composite microbelts, as a contrast sample, were also fabricated by mixing spinning solution S_{a4} and spinning solution S_{b2} together at the volume ratio of 1:1 and electrospun using traditional single-spinneret electrospinning method to study the superiority of the structure of belt-shaped coaxial microcables. The other spinning parameters were the same as they were in the fabrication of belt-shaped coaxial microcables.

Characterizations

The as-prepared Fe_3O_4 NPs and $[Fe_3O_4/PANI/PMMA]$@{$[Eu(BA)_3phen+Tb(BA)_3phen]$/PMMA} belt-shaped coaxial microcables were examined by X-ray powder diffractometer (XRD, D8 FOCUS, Bruker, Switzerland, Germany) with Cu Ka radiation (λ= 0.15406 nm) and Ni filter, the operation current and voltage were maintained at 20 mA and 40 kV, and scanning speed, step length and diffraction range were settled as 10 ° min^{-1}, 0.1 ° and 10-80 °, respectively. The morphology and size of Fe_3O_4 NPs were observed by a transmission electron

microscope (TEM, Jeol, JEM-2010, Tokyo, Japan). The belt-shaped coaxial microcables were observed by a field emission scanning electron microscope (FESEM, Philips, XL-30 SFEG, Eindhoven, Netherlands) equipped with an energy-dispersive X-ray spectrometer (EDS). The internal structure of the belt-shaped coaxial microcable was observed by a biological microscope (BM, CVM500E, Beijing, China). The measures of photoluminescence (PL) spectra and the luminescence decay curves were performed by a fluorescence spectrophotometer (Hitachi, F-7000, Tokyo, Japan) using a 150 W Xe lamp as the excitation source, and scanning speed was fixed at 1200 nm·min^{-1}. Then, the magnetic performance of Fe_3O_4 NPs and belt-shaped coaxial microcables was measured by a vibrating sample magnetometer (VSM, Quantum Design, MPMS SQUID XL, San Diego, California, America). The conductive property was detected by Hall effect measurement system (Ecopia, HMS-3000, Kyungki-Do Korea). The ultraviolet-visible spectra of samples were determined by a ultraviolet-visible spectrophotometer (Shimadzu, UV-1240, Kyoto, Japan). Fourier transform infrared spectrum of the core solution was determined by a Fourier transform infrared spectrometer (FTIR, Shimadzu, 8400S, Kyoto, Japan). All the measures were performed at room temperature.

3 Results and discussion

3.1 Characterizations of the structure and morphology

The phase compositions of the Fe_3O_4 NPs and [Fe_3O_4/PANI/PMMA]@{[Eu(BA)$_3$phen+Tb(BA)$_3$phen]/PMMA} belt-shaped coaxial microcables were identified by means of XRD analysis, as shown in Figure 2. It is obvious that all the diffraction peaks of Fe_3O_4 NPs are in agreement with those of cubic magnetite (PDF 88-0315) and no other phases or impurities can be detected. From the XRD analysis result of the belt-shaped coaxial microcables, the Fe_3O_4 NPs are completely incorporated into belt-shaped coaxial microcables. Moreover, the diffraction intensities of Fe_3O_4 in the belt-shaped coaxial microcables are weaker than those of the Fe_3O_4 NPs because of the existence of PANI, rare earth complexes and PMMA. The diffraction peaks of the amorphous PMMA (2θ≈ 15°)[42] and PANI (2θ≈ 22°)[43] could also be observed. The XRD patterns of Fe_3O_4/[Eu(BA)$_3$phen+Tb(BA)$_3$phen]/PANI/PMMA composite microbelts are similar to those of the belt-shaped coaxial microcables.

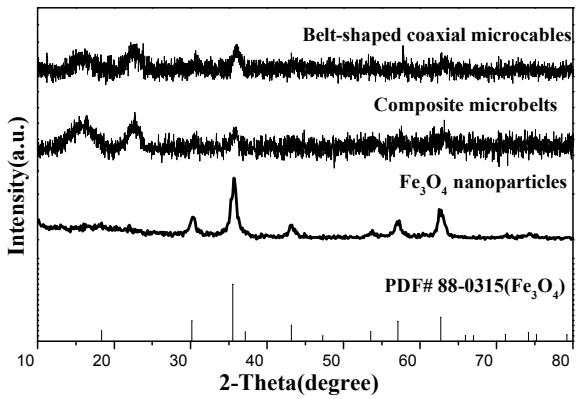

Figure 2 XRD patterns of Fe_3O_4 NPs, [Fe_3O_4/PANI/PMMA]@{[Eu(BA)$_3$phen+Tb(BA)$_3$phen]/PMMA} belt-shaped coaxial microcables (S_{a4}@S_{b2}) and composite microbelts with PDF standard card of Fe_3O_4 NPs.

The morphology of the as-prepared Fe_3O_4 NPs was observed by means of TEM, as presented in Figure 3A. The size distribution of the spherical Fe_3O_4 NPs is almost uniform, and the particle size of the Fe_3O_4 NPs is 9.85±0.085 nm (Figure 3B). The morphology and structure of [Fe_3O_4/PANI/PMMA]@{[Eu(BA)$_3$phen+Tb(BA)$_3$phen]/PMMA} belt-shaped coaxial microcables (S_{a4}@S_{b2}) were characterized by the combination of SEM, biological microscopy (BM) and EDS line-scan. The SEM image of [Fe_3O_4/PANI/PMMA]@{[Eu(BA)$_3$phen+Tb(BA)$_3$phen]/PMMA} belt-shaped coaxial microcables shown in Figure 3C demonstrates that the structure of belt-shaped coaxial microcables was successfully prepared. The surface of the belt-shaped coaxial microcables is smooth, the width of the belt-shaped coaxial microcables is 14.369±0.169 μm (Figure 3D) and the thickness is about 2.77 μm. As seen in the SEM image (Figure 3C), all the broadsides of these belt-shaped microcables are facing up, with few exceptions, which probably because the belt-shaped coaxial microcables lay in a more stable and lower potential energy state onto the iron net.

As revealed in Figure 3E, an obvious coaxial structure of the belt-shaped coaxial microcable is observed, which is composed of a dark-colored core and a light-colored shell. It is remarkably noticed that the Fe_3O_4 NPs are uniformly dispersed in the core of the belt-shaped coaxial microcables.

EDS line-scan analysis is performed in order to further confirm the structure of belt-shaped coaxial microcables. As shown in Figure 3F, Tb, Eu, S and Fe elements represent Tb(BA)$_3$phen, Eu(BA)$_3$phen, CSA doped PANI and Fe_3O_4, respectively. Elemental Fe and S exist in the middle domain of the [Fe_3O_4/PANI/PMMA]@{[Eu(BA)$_3$phen+Tb(BA)$_3$phen]/PMMA} belt-shaped coaxial microcables. The amounts of elemental Tb and Eu in the middle domain of the belt-shaped coaxial microcables are lower than those in both sides of the belt-shaped coaxial microcables because Tb(BA)$_3$phen, Eu(BA)$_3$phen merely exist in the top and bottom surfaces of the middle domain of the belt-shaped coaxial microcables. It is further found that elemental Tb and Eu without elemental Fe and S are dispersed in both sides of the belt-shaped coaxial microcables. These results are consistent with the core-shell structure of belt-shaped coaxial microcables. By the analyses of SEM, BM and EDS line-scan, we can safely draw a conclusion that [Fe_3O_4/PANI/PMMA]@{[Eu(BA)$_3$phen+Tb(BA)$_3$phen]/PMMA} belt-shaped coaxial microcables have been successfully prepared.

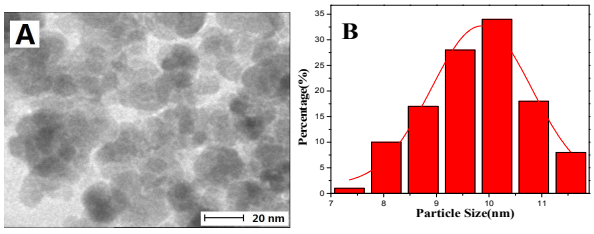

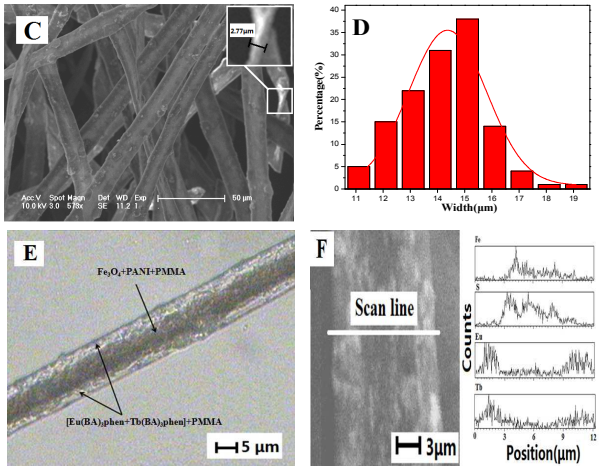

Figure 3 SEM image (A) and histogram of particle size of Fe_3O_4 NPs (B), SEM image (C), histogram of width (D), BM images(E) and EDS line-scan analysis (F) of belt-shaped coaxial microcables ($S_{a4}@S_{b2}$).

3.2 Photoluminescence property

Photoluminescence properties of the belt-shaped coaxial microcables with different mass ratios of $Eu(BA)_3phen$ to $Tb(BA)_3phen$ (samples $S_{ax}@S_{b2}$, x= 1-7) were investigated to study the color tunable property, while the mass percentage of PANI to PMMA was settled as 30 % and the mass ratio of Fe_3O_4 to PMMA was fixed as 3:1. The excitation spectra were monitored at 545 nm and 615 nm, while the emission spectra were measured with 281 nm as the excitation wavelength, as shown in Figure 4 and Figure 5. The excitation spectra (Figure 4A, 4B) consist of a broad excitation band extending from 200 to 350 nm with a maximum at 281 nm in the wavelength region, which is attributed to the $\pi \rightarrow \pi^*$ electron transition of the conjugated double bonds of the ligand. The excitation intensity is increased with introducing more $Tb(BA)_3phen$ when monitored at 545 nm (Figure 4A), while the excitation intensity is increased with the increase of Eu^{3+} ion concentration (Figure 4B) when the monitoring wavelength is 615 nm.

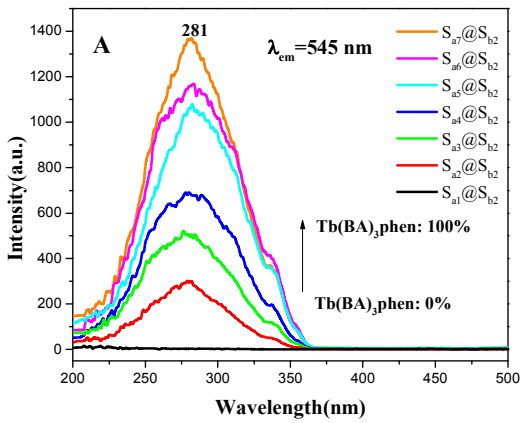

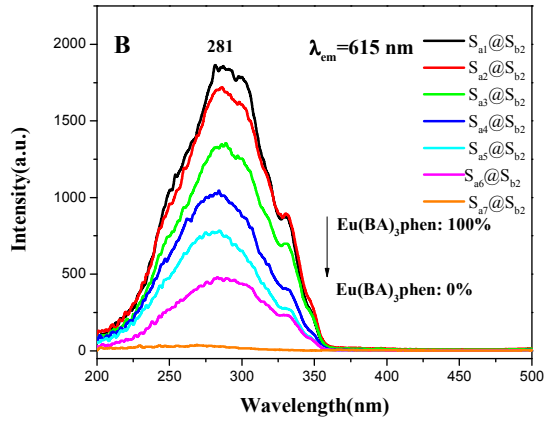

Figure 4 Excitation spectra of samples $S_{ax}@S_{b2}$ (x= 1-7) monitored at 545 nm (A) and 615 nm (B).

The emission spectra of belt-shaped coaxial microcables show peaks at 490 and 545 nm due to the $^5D_4 \rightarrow {}^7F_J$ (J= 6, 5) transitions of Tb^{3+}, and peaks at 592 and 615 nm ascribed to the $^5D_0 \rightarrow {}^7F_J$ (J= 1, 2) transitions of Eu^{3+} (shown in Figure 5A). One can see that with the decrease of the mass ratio of $Eu(BA)_3phen$ to $Tb(BA)_3phen$, the green fluorescence emissions at 490 and 545 nm of Tb^{3+} ions enhance gradually, while the orange and red fluorescence emissions at 592 and 615 nm of Eu^{3+} ions gradually decrease. In order to clearly depict the variation trend, the intensities of the characteristic emission peaks of each sample versus different samples were plotted in the Figure 5B. The variation of the PL intensity of the Eu^{3+} and Tb^{3+} can be attributed to the energy distribution. Since the energy that the matrix absorbs and the content of $RE(BA)_3phen$ (RE= Eu and Tb) are constant, more energy is assigned to Eu^{3+} with the increase of $Eu(BA)_3phen$ content, thus leading to stronger fluorescence peaks at 592 and 615 nm. Meanwhile, on the contrary, the energy assigned to Tb^{3+} is reduced and the fluorescence peaks at 481 and 545 nm are weakened. Therefore, it is evidently found that the emission spectra of belt-shaped coaxial microcables could be tuned by adjusting the mass ratio of $Eu(BA)_3phen$ and $Tb(BA)_3phen$ complexes in the belt-shaped coaxial microcables.

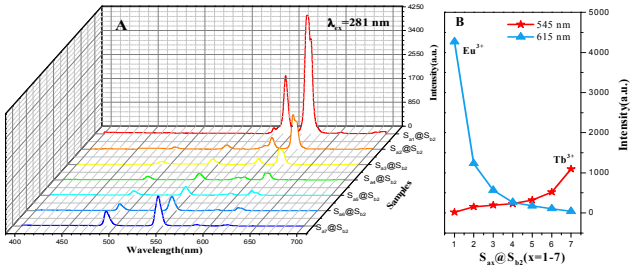

Figure 5 Emission spectra of samples $S_{ax}@S_{b2}$ (x= 1-7) when the mass percentage of PANI is fixed as 30 % and the mass ratio of Fe_3O_4 to PMMA is fixed as 3:1 (A), dependence of the emission intensity on the various samples (B).

It offers an approach to tune emission colors by adjusting the mass ratio of $Eu(BA)_3phen$ to $Tb(BA)_3phen$ complexes in the belt-shaped coaxial microcables. Chromaticity coordinates of the Commission Internationale de L'Eclairage (CIE) are studied. The CIE chromaticity coordinates for belt-shaped coaxial microcables excited at 281 nm are represented in the CIE diagram of Figure

6A with the data given in Table 3. It can be observed that the luminescence color can be tuned from red to green by adjusting the mass ratios of $Eu(BA)_3phen$ complexes to $Tb(BA)_3phen$ complexes. The corresponding photographs of the tunable colors generated from those belt-shaped coaxial microcables excited with 281 nm UV lamps are shown in Figure 6B.

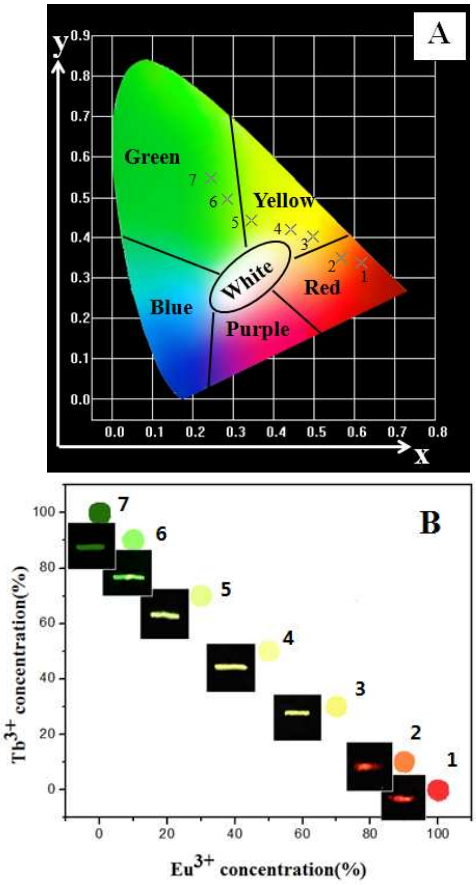

Figure 6 CIE chromaticity coordinates diagram of samples $S_{ax}@S_{b2}$ (x= 1-7) (A) and the corresponding luminescence photographs under the excitation of 281-nm ultraviolet light (B).

Table 3 CIE Chromaticity Coordinates for samples $S_{ax}@S_{b2}$ (x= 1-7)

Lables	Samples	Concentration	CIE(x, y)
1	$S_{a1}@S_{b2}$	100 %Eu, 0 %Tb	(0.618,0.338)
2	$S_{a2}@S_{b2}$	90 %Eu, 10 %Tb	(0.568,0.350)
3	$S_{a3}@S_{b2}$	70 %Eu, 30 %Tb	(0.498,0.403)
4	$S_{a4}@S_{b2}$	50 %Eu, 50 %Tb	(0.442,0.421)
5	$S_{a5}@S_{b2}$	30 %Eu, 70 %Tb	(0.344, 0.442)
6	$S_{a6}@S_{b2}$	90 %Eu, 10 %Tb	(0.286,0.494)
7	$S_{a7}@S_{b2}$	0 %Eu, 100 %Tb	(0.246,0.548)

The photoluminescence lifetime curves of Tb^{3+} emission at 545 nm and Eu^{3+} emission at 615 nm in belt-shaped coaxial microcables under the excitation of 281-nm ultraviolet light are shown in Figure 7, respectively. It is found that the curves follow the single-exponential decay:

$$I_t = I_0 \exp(-t/\tau)$$

where I_t is the intensity at time t, I_0 is the intensity at t= 0, t is the decay time and τ is the lifetime. From Figure 7, the fluorescence lifetime values of Tb^{3+} gradually decrease with increasing in Tb^{3+} concentration and decreasing in Eu^{3+} concentration. It reveals the same conclusion that lifetime of Eu^{3+} ions diminishes with decreasing in $Tb(BA)_3phen$ complexes and increasing in Eu^{3+} concentration. The possible reasons for this result are as follows. The content of $Tb(BA)_3phen$ complex in the belt-shaped coaxial microcables is reduced, while the content of $Eu(BA)_3phen$ is increased. Thus the distance among Tb^{3+} in $Tb(BA)_3phen$ molecular clusters and/or nanoparticles in the belt-shaped coaxial microcables is increased, resulting in that the energy transfer among Tb^{3+} to Tb^{3+} is reduced and the fluorescence lifetime of Tb^{3+} is prolonged. On the other hand, more aggregates of $Eu(BA)_3phen$ are formed in the polymer matrix with introducing more $Eu(BA)_3phen$. The exciton migration between the $Eu(BA)_3phen$ molecules shortens the fluorescence lifetime of Eu^{3+}[42].

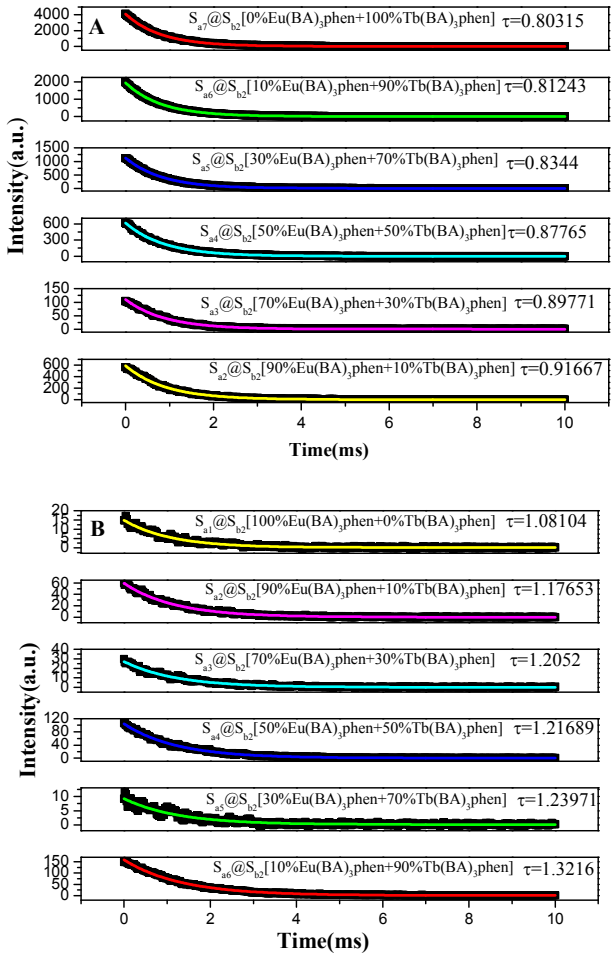

Figure 7 Lifetime curves of Tb^{3+} (A) and Eu^{3+} (B) in samples $S_{ax}@S_{b2}$ (x= 1-7).

Besides, the fluorescent properties of the [Fe_3O_4/PANI/PMMA]@[50%$Eu(BA)_3phen$+50%$Tb(BA)_3phen$]/PMMA belt-shaped coaxial microcables with different PANI contents ($S_{a4}@S_{b2}$, $S_{a4}@S_{b4}$ and $S_{a4}@S_{b5}$) are also investigated. The mass ratio of Fe_3O_4 NPs to PMMA is fixed at 3:1. As shown in Figure 8(A, B, C), it is clearly observed that emission and excitation intensity decrease with the increase of the PANI

content. From the UV-Vis absorption spectrum of PANI illustrated in Figure 8D, it can be seen that the PANI can absorb visible light (400-700 nm) and much more easily absorb the ultraviolet light (<400 nm). Moreover, as shown in Figure 8D, a broad absorption peak around 615 nm is also observed, meaning that PANI absorbs red light much stronger. The exciting light and emitting light in the belt-shaped coaxial microcables are absorbed by PANI, resulting in that the intensities of exciting light and emitting light are decreased, and the light absorption becomes stronger with introducing more PANI into the belt-shaped coaxial microcables.

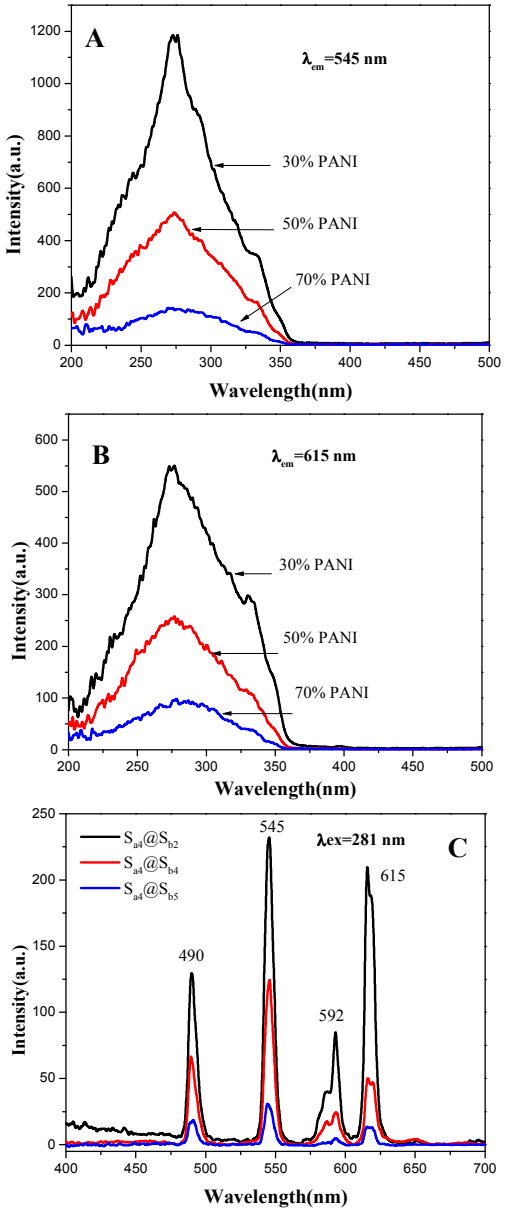

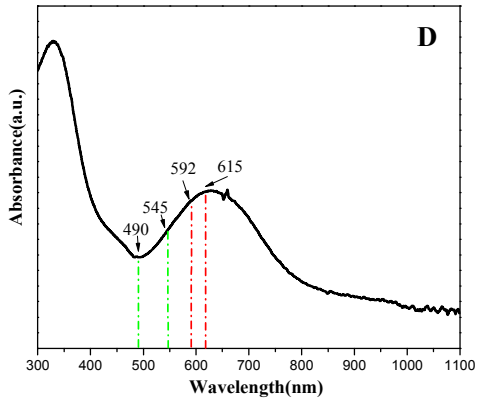

Figure 8 Excitation spectra (A, B), emission spectrum (C) of belt-shaped coaxial microcables containing different mass percentages of PANI and UV-Vis absorbance spectrum of PANI/PMMA (D).

The CIE chromaticity coordinates for the samples and their corresponding photographs upon excitation at 281-nm ultraviolet light are provided in the Figure 9. It demonstrates that the emitting color of belt-shaped coaxial microcables becomes more green with introducing more PANI, due to the stronger absorption of red light by PANI.

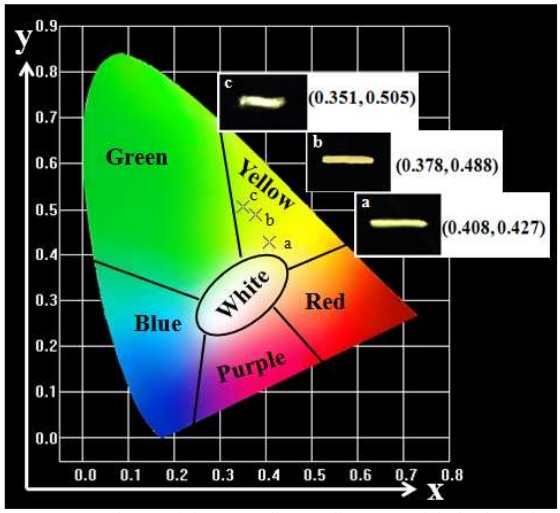

Figure 9 CIE chromaticity coordinate diagram of belt-shaped coaxial microcables containing different mass percentages of PANI.

Meanwhile, the [Fe_3O_4/PANI/PMMA]@{[50%Eu(BA)$_3$phen+50%Tb(BA)$_3$phen]/PMMA} belt-shaped coaxial microcables containing different amounts of Fe_3O_4 NPs were fabricated to research the effect of adding different contents of Fe_3O_4 NPs (samples $S_{a4}@S_{b1}$, $S_{a4}@S_{b2}$, $S_{a4}@S_{b3}$, as illustrated in Figure 10) on the fluorescent properties of the belt-shaped coaxial microcables. Similarly, the excitation and emission intensity of belt-shaped coaxial microcables are decreased with the increase of Fe_3O_4 NPs content. This phenomenon can be explained as the light absorption of Fe_3O_4 NPs. From the absorbance spectrum of Fe_3O_4 NPs illustrated in Figure 10D, it is seen that the Fe_3O_4 NPs can absorb light at ultraviolet wavelength (<400 nm) much more strongly than visible range (400-700 nm). The exciting light and emitting light in the belt-shaped coaxial microcables are absorbed by Fe_3O_4 NPs, leading to the fact that the intensities of exciting light

and emitting light are decreased, and the light absorption becomes stronger with introducing more Fe_3O_4 NPs into the belt-shaped coaxial microcables.

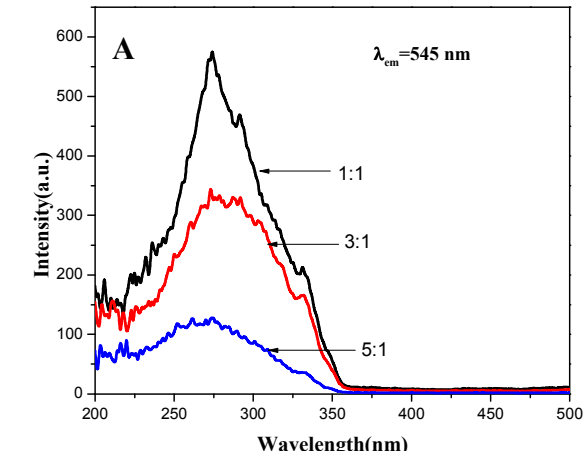

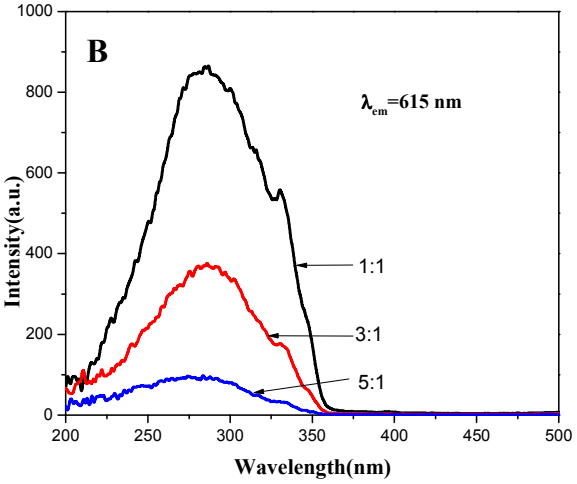

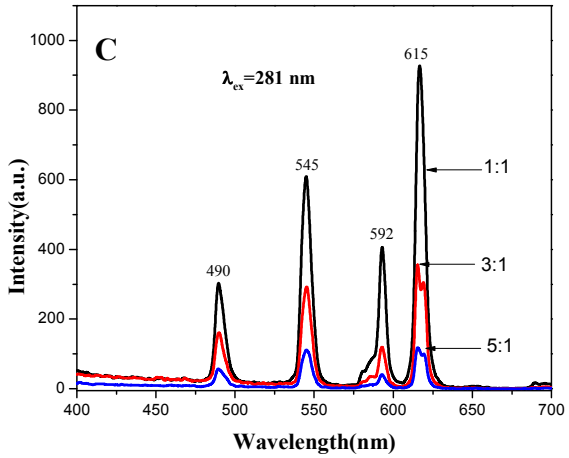

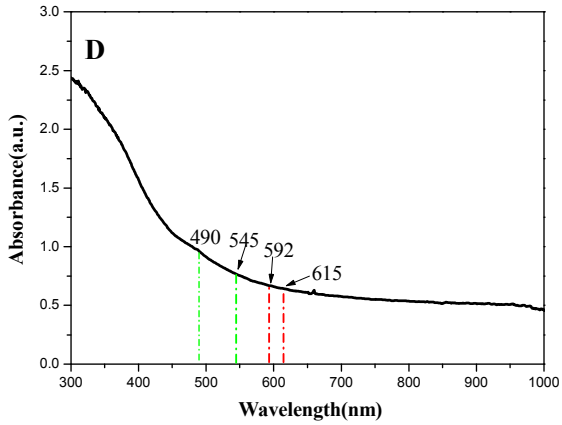

Figure 10 Excitation spectra (A, B), emission spectrum (C) of belt-shaped coaxial microcables containing different mass ratios of Fe_3O_4 and UV-Vis absorbance spectrum of Fe_3O_4 NPs (D).

Figure 11 is the CIE coordinate diagram of belt-shaped coaxial microcables with different Fe_3O_4 contents under the excitation of 281-nm ultraviolet light. It demonstrates that the emitting color of the belt-shaped coaxial microcables becomes more red with introducing more Fe_3O_4, which can be attributed to the fact that Fe_3O_4 has stronger light absorption for the light at ultraviolet range.

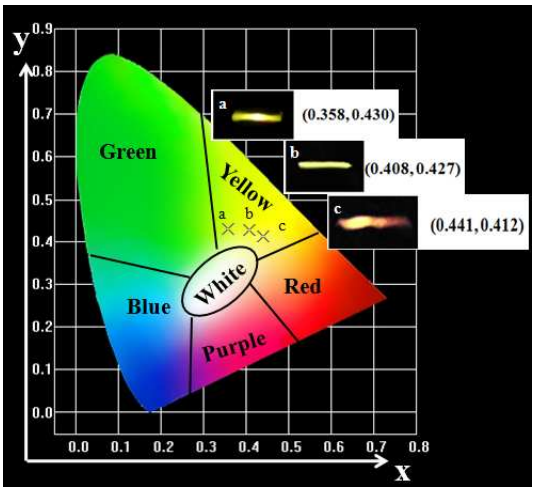

Figure 11 CIE chromaticity coordinate diagram of belt-shaped coaxial microcables containing different mass ratios of Fe_3O_4.

From the contrast between the belt-shaped coaxial microcables (S_{a4}@S_{b2}) and Fe_3O_4/[$Eu(BA)_3$phen+$Tb(BA)_3$phen]/PANI/PMMA composite microbelts, as shown in Figure 12, one can see that excitation and emission intensity of the belt-shaped coaxial microcables are much stronger than those of Fe_3O_4/[$Eu(BA)_3$phen+$Tb(BA)_3$phen]/PANI/PMMA composite microbelts. This result can be attributed to the isolation of [$Eu(BA)_3$phen+$Tb(BA)_3$phen] from Fe_3O_4 NPs and PANI. As illustrated in Figure 13, [$Eu(BA)_3$phen+$Tb(BA)_3$phen], Fe_3O_4 NPs and PANI are promiscuously dispersed in the Fe_3O_4/[$Eu(BA)_3$phen+$Tb(BA)_3$phen]/PANI/PMMA composite microbelts. The exciting light in the composite microbelts has to pass through Fe_3O_4 NPs and PANI to reach and excite

RE(BA)$_3$phen (RE= Eu, Tb). In this process, a large part of the exciting light has been absorbed by Fe_3O_4 NPs and PANI, and thus the exciting light is much weakened before it reaches the RE(BA)$_3$phen (RE= Eu, Tb). Similarly, the emitting light emitted by RE(BA)$_3$phen (RE= Eu, Tb) also has to pass through Fe_3O_4 NPs and PANI and is absorbed by them. Consequently, both the exciting and emitting light are severely weakened. For the belt-shaped coaxial microcables, Fe_3O_4 NPs and PANI are separated from Eu(BA)$_3$phen and Tb(BA)$_3$phen complexes in their own domains of the belt-shaped coaxial microcables, so that the exciting light and emitting light in the {[Eu(BA)$_3$phen+Tb(BA)$_3$phen]/PMMA} domain will almost be unaffected by Fe_3O_4 NPs and PANI. The overall result is that the belt-shaped coaxial microcables possess much higher fluorescent performance than the Fe_3O_4/[Eu(BA)$_3$phen+Tb(BA)$_3$phen]/PANI/PMMA composite microbelts. Thus, a strong fluorescent emission intensity of the belt-shaped coaxial microcables is achieved by isolating Eu(BA)$_3$phen and Tb(BA)$_3$phen from Fe_3O_4 NPs and PANI.

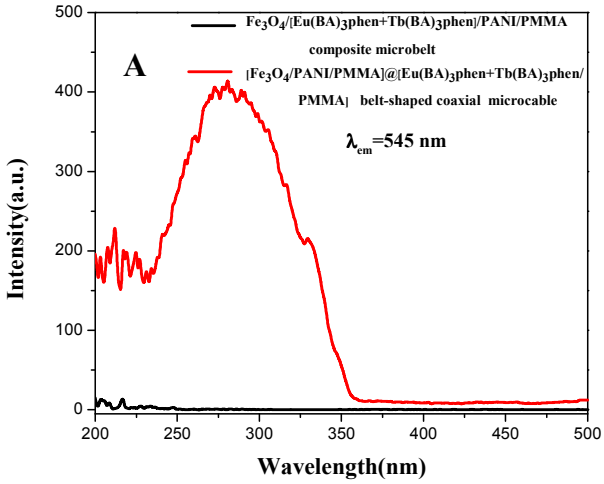

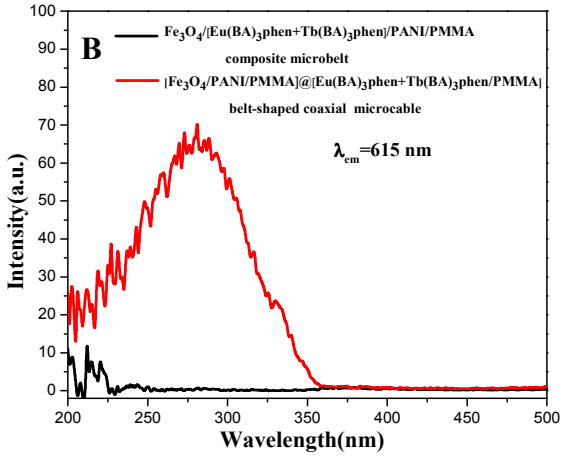

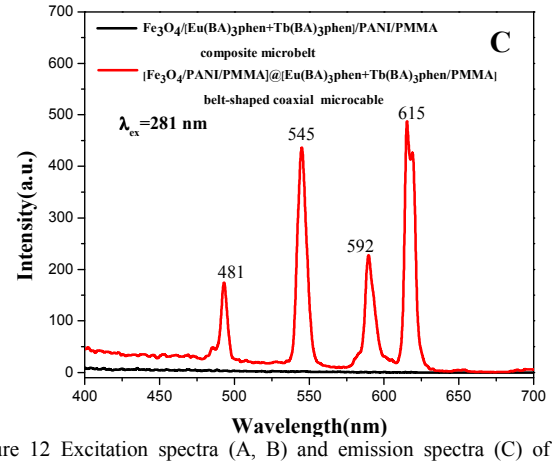

Figure 12 Excitation spectra (A, B) and emission spectra (C) of belt-shaped coaxial microcables (S_{a4}@S_{b2}) and Fe_3O_4/[Eu(BA)$_3$phen+Tb(BA)$_3$phen]/PANI/PMMA composite microbelts.

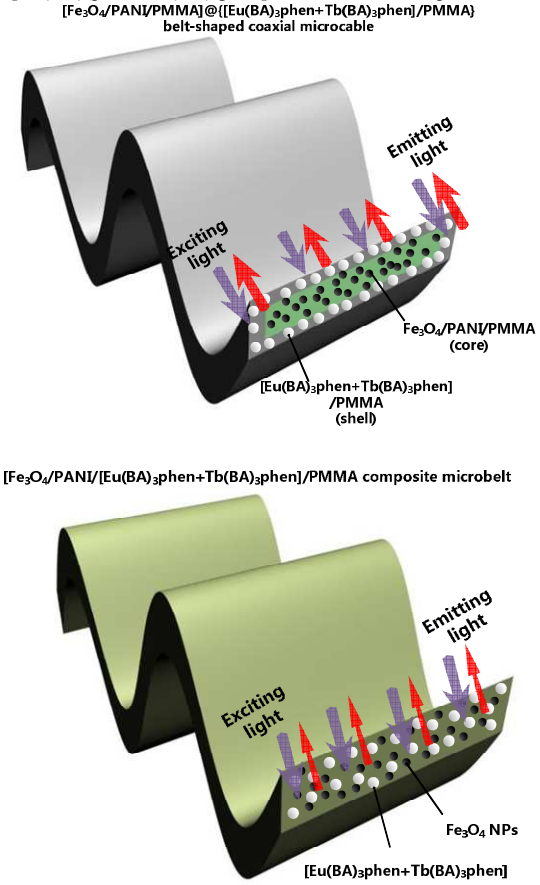

Figure 13 Schematic diagrams of the situation of the exciting light and emitting light in the Fe_3O_4/[Eu(BA)$_3$phen+Tb(BA)$_3$phen]/PANI/PMMA composite microbelt and [Fe_3O_4/PANI/PMMA]@{[Eu(BA)$_3$phen+Tb(BA)$_3$phen]/PMMA} belt-shaped coaxial microcable.

3.3 Electrical conductivity analysis

As a result of conductive PANI in the core of [Fe_3O_4/PANI/PMMA]@{[Eu(BA)$_3$phen+Tb(BA)$_3$phen]/PMMA} belt-shaped coaxial microcables, the belt-shaped coaxial microcables are insulated from others. The electrical conductivity values of the cores we used for the [Fe_3O_4/PANI/PMMA]@{[Eu(BA)$_3$phen+Tb(BA)$_3$phen]/PMMA} belt-shaped coaxial microcables are summarized in Table 4

through measuring the dried spinning solution II-S_{b2} (30 %), II-S_{b4} (50 %) and II-S_{b5} (70 %). The conductivities of these microstructures can be tuned by adjusting the mass percentage of PANI to PMMA. Obviously, the more PANI introduced into the cores, the higher electrical conductivity of the cores, as PANI is consecutive in the Fe_3O_4/PANI/PMMA microbelts and probably forms the conducting network more easily, which render more efficient charge transport.

Table 4 Electrical conductivity and resistivity of the cores doped with various amount of PANI

Spinning solution II	Conductiviy (S·cm^{-1})	Resistivity (Ω·cm)
S_{b2}	5.47×10^{-4}	1.827×10^{3}
S_{b4}	1.44×10^{-3}	6.96×10^{2}
S_{b5}	2.63×10^{-2}	3.8×10^{1}

The influences of cores of the different mass ratios of Fe_3O_4 on electrical conductivity were also investigated by measuring the dried spinning solution II-S_{b1} (1:1), II-S_{b2} (3:1) and II-S_{b3} (5:1). The electrical conductivity values were summarized in Table 5. It is found from Table 5 that the conductivity of the spinning solution II is decrease with increasing in the mass ratios of Fe_3O_4, as a result of some influence of Fe_3O_4 NPs on the polymerization process of aniline. It cannot form the conducting network more easily, which hinder efficient charge transport.

Table 5 Electrical conductivity and resistivity of the cores doped with different mass ratios of Fe_3O_4

Spinning solution II	Conductiviy (S·cm^{-1})	Resistivity (Ω·cm)
S_{b1}	5.53×10^{-4}	1.881×10^{3}
S_{b2}	5.47×10^{-4}	1.827×10^{3}
S_{b3}	5.28×10^{-4}	1.894×10^{3}

In order to investigate the insulativity of each belt-shaped coaxial microcables, the surface conductivities of the belt-shaped coaxial microcables which were fabricated by using the spinning solution II-S_{b2} (30 %), II-S_{b4} (50 %) and II-S_{b5} (70 %), were also measured by Hall effect measurement system. The results (Table 6) reveal that the surface conductivity of all the belt-shaped coaxial microcables are lower than the order of 10^{-10} S·cm^{-1}, indicating that the belt-shaped coaxial microcables are well insulated.

Table 6 Electrical conductivity and resistivity of the samples doped with various amount of PANI

Samples	Conductiviy (S·cm^{-1})	Resistivity (Ω·cm)
S_{a4}@S_{b2}	3.32×10^{-10}	3.012×10^{9}
S_{a4}@S_{b4}	6.43×10^{-10}	1.555×10^{9}
S_{a4}@S_{b5}	8.40×10^{-10}	1.190×10^{9}

3.4 Magnetic property

The typical hysteresis loops for Fe_3O_4 NPs, and [Fe_3O_4/PANI/PMMA]@{[Eu(BA)$_3$phen+Tb(BA)$_3$phen]/PMMA} belt-shaped coaxial microcables containing various mass ratios of Fe_3O_4 NPs measured at room temperature are shown in Figure 14.

It is a well-known fact that the saturation magnetization of a magnetic composite material depends on the mass percentage of the magnetic substance in the magnetic composite material. It is found from Table 7 that the saturation magnetization of the belt-shaped coaxial microcables is increased from 6.38 emu·g^{-1} to 21.51 emu·g^{-1} with the increase of Fe_3O_4 NPs.

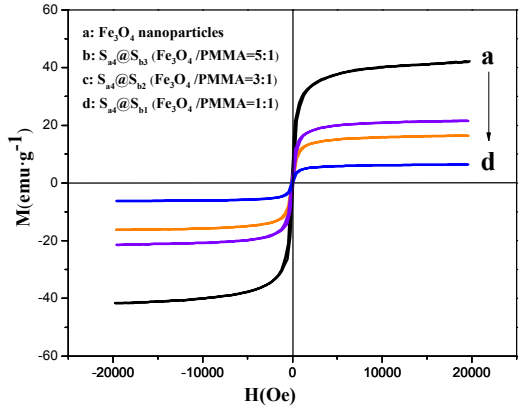

Figure 14 Hysteresis loops of Fe_3O_4 NPs, and [Fe_3O_4/PANI/PMMA]@{[Eu(BA)$_3$phen+Tb(BA)$_3$phen]/PMMA} belt-shaped coaxial microcables.

Table 7 Saturation magnetization of Fe_3O_4 NPs, and [Fe_3O_4/PANI/PMMA]@{[Eu(BA)$_3$phen+Tb(BA)$_3$phen]/PMMA} belt-shaped coaxial microcables

Samples	Saturation magnetization (Ms)/emu·g^{-1}
Fe_3O_4 NPs	42.17
S_{a4}@S_{b1} (Fe_3O_4 : PMMA= 1:1)	6.38
S_{a4}@S_{b2} (Fe_3O_4 : PMMA= 3:1)	16.33
S_{a4}@S_{b3} (Fe_3O_4 : PMMA= 5:1)	21.51

4 Conclusions

By one-pot electrospinning, the tuned magnetism, electricity and fluorescent color trifunctional belt-shaped coaxial microcables are successfully prepared. Every belt-shaped coaxial conductive microcable consists of a Fe_3O_4/PANI/PMMA conductive-magnetic bifunctional core and a [Eu(BA)$_3$phen+Tb(BA)$_3$phen]/PMMA insulating photoluminescent shell, so that belt-shaped coaxial microcables are insulated from each other. The emitting color of the belt-shaped coaxial microcables can be tuned in a wide color range of red-yellow-green by adjusting the mass ratio of europium complexes, terbium complexes, PANI content, or Fe_3O_4 NPs content. Meanwhile, the conductivity and magnetism of the belt-shaped coaxial microcables can be tunable by adjusting the contents of PANI and Fe_3O_4 NPs. The adopted conditions can produce stable and convenient microcables. In addition, it is found from our attempt that when the mass percentage of PANI to PMMA, and the mass ratio of Fe_3O_4 to PMMA exceed 70 % and 6:1 respectively, it cannot produce stable and convenient microcables due to the formation of unstable or over highly viscous spinning solutions. This microstructure is ideally suited to be applied in high density electrical connections in narrow spaces, such as in mobile phones, subminiature integrated circuits, microchips and nano/micromachines.

Acknowledgment

This work was financially supported by the National Natural Science Foundation of China (NSFC 50972020, 51072026), Specialized Research Fund for the Doctoral Program of Higher Education (20102216110002,20112216120003), the Science and Technology Development Planning Project of Jilin Province (Grant Nos. 20130101001JC, 20070402, 20060504), the Research Project of Science and Technology of Department of Education of Jilin Province "11th 5-year plan" (Grant Nos. 2010JYT01), Key Research Project of Science and Technology of Ministry of Education of China (Grant No. 207026).

Notes and references

Key Laboratory of Applied Chemistry and Nanotechnology at Universities of Jilin Province, Changchun University of Science and Technology, Changchun 130022. Fax: 86 0431 85383815; Tel: 86 0431 85582574; E-mail: dongxiangting888@163.com

1. Y. R. Weng, J. Zhao, S. Y. Yu and S. Y. Song, *CrystEngComm*, 2014, **16**, 6257.
2. Y. Gong, J. W. Dai, H. Li, X. Wang, H. R. Xiong, Q. Y. Zhang, P. H. Li, C. F. Yi, Z. S. Xu, H. B. Xu and P. K. Chu, *J. Biomater. Appl.*, 2015, DOI: 10.1177/0885328215575761, 1.
3. J. M. Rankin, N. K. Neelakantan, K. E. Lundberg, E. M. Grzincic, C. J. Murphy and K. S. Suslick, *Adv. Sci.*, 2015, DOI: 10.1002/advs.201500114, 1.
4. Z. C. Guo, C. L. Shao, M. Y. Zhang, J. B. Mu, Z. Y. Zhang, P. Zhang, B. Chen and Y. C. Liu, *J. Mater. Chem.*, 2011, **21**, 12083.
5. S. Y. Yu, X. C. Gao, H. Jing, R. F. Zhang, X. L. Gao and H. Q. Su, *CrystEngComm*, 2014, **16**, 6645.
6. T. Liu, X. W. Liu, Y. J. Yao, J. Zhou, J. Zhu, G. Sun and D. N. He, *RSC Adv.*, 2015, **5**, 24049.
7. S. Rittikulsittichai, B. Singhana, W. W. Bryan, S. Sarangi, A. C. Jamison, A. Brazdeikis and T. R. Lee, *RSC Adv.*, 2013, **3**, 7838.
8. M. Bayat, H. Yang, F. K. Ko, D. Michelson and A. Mei, *Polymer*, 2014, **55**, 936.
9. D. Q. Zhang, J. Y. Cheng, X. Y. Yang, B. Zhao and M. S. Cao, *J. Mater. Sci.*, 2014, **49**, 7221.
10. S. C. Wuang, K. G. Neoh, E.-T. Kang, D. W. Pack and D. E. Leckband, *J. Mater. Chem.*, 2007, **17**, 3354.
11. Q. A. Pankhurst, J. Connolly, S. K. Jones and J. Dobson, *J. Phys. D: Appl. Phys.*, 2003, **36**, 167.
12. D. H. Zhang and Y. Y. Wang, *Mater. Sci. Eng. B*, 2006, **134**, 9.
13. S. Virji, R. B. Kaner and B. H. Weiller, *Chem. Mater.*, 2005, **17**, 1256.
14. Q. H. Zhang, H. F. Jin, X. H. Wang and X. B. Jing, *Synth. Met.*, 2001, **123**, 481.
15. Q. L. Ma, W. S. Yu, X. T. Dong, J. X. Wang, G. X. Liu and J. Xu, *J. Nanopart. Res.*, 2012, **14**, 1203.
16. H. G. Wang, Y. X. Li, L. Sun, Y. C. Li, W. Wang, S. Wang, S. F. Xu and Q. B. Yang, *J. Colloid Interf. Sci.*, 2010, **350**, 396.
17. Q. L. Ma, W. S. Yu, X. T. Dong, J. X. Wang, G. X. Liu and J. Xu, *Opt. Mater.*, 2013, **35**, 526.
18. S. J. Sheng, Q. L. Ma, X. T. Dong, N. Lv, J. X. Wang, W. S. Yu and G. X. Liu, *Luminescence*, 2015, **30**, 26.
19. S. J. Sheng, Q. L. Ma, X. T. Dong, N. Lv, J. X. Wang, W. S. Yu and G. X. Liu, *J. Mater. Sci: Mater. Electron.*, 2014, **25**, 1309.
20. S. J. Sheng, Q. L. Ma, X. T. Dong, N. Lv, J. X. Wang, W. S. Yu and G. X. Liu, *J. Mater. Sci: Mater. Electron.*, 2014, **25**, 2279.
21. K. Lun, Q. L. Ma, M. Yang, X. T. Dong, Y. Yang, J. X. i. Wang, W. S. Yu and G. X. Liu, *Chem. Eng. J.* , 2015, **279**, 231.
22. Y. S. Zhao, H. Fu, F. Hu, A. D. Peng and J. Yao, *Adv. Mater.*, 2007, **19**, 3554.
23. C. M. Zhang and J. Lin, *Chem. Soc. Rev.*, 2012, **41**, 7938.
24. Z. L. Liu, L. X. Yu, Q. Wang, Y. C. Tao and H. Yang, *J. Lumin.*, 2011, **131**, 12.
25. Y. B. Zeng, Z. Q. Li, L. M. Wang and Y. J. Xiong, *CrystEngComm*, 2012, **14**, 7043.
26. A. Zahoor, Q. Teng, H. Q. Wang, M. A. Choudhry and X. Y. Li, *Met. Mater. Int.*, 2011, **17**, 417.
27. M. Miyauchi, J. Miao, T. J. Simmons, J.-W. Lee, T. V. Doherty, J. S. Dordick and R. J. Linhardt, *Biomacromolecules*, 2010, **11**, 2440.
28. G. W. She, X. H. Zhang, W. S. Shi, Y. Cai, N. Wang, P. Liu and D. M. Chen, *Cryst. Growth Des.*, 2008, **8**, 1789.
29. S. Kumar, V. Kundu, A. Vohra and S. K. Chakarvarti, *J. Mater. Sci.: Mater. Electron.*, 2011, **22**, 995.
30. T. H. Han, W. J. Lee, D. H. Lee, J. E. Kim, E.-Y. Choi and S. O. Kim, *Adv. Mater.*, 2010, **22**, 2060.
31. J. Song, M. L. Chen, M. B. Olesen, C. X. Wang, R. Havelund, Q. Li, E. Q. Xie, R. Yang, P. Boggild, C. Wang, F. Besenbacher and M. D. Dong, *Nanoscale*, 2011, **3**, 4966.
32. Q. L. Ma, J. X. Wang, X. T. Dong, W. S. Yu and G. X. Liu, *RSC Adv.*, 2015, **5**, 2523.
33. D. L. Shi, M. E. Sadat, A. W. Dunn and D. B. Mast, *Nanoscale*, 2015, **7**, 8209.
34. G. N. Wang, L. Jin, Y. K. Dong, L. Niu, Y. X. Liu, F. Ren and X. G. Su, *New J. Chem.*, 2014, **38**, 700.
35. Q. L. Yang, J. Zhai, Y. L. Song, M. X. Wan, L. Jiang, W. G. Xu and Q. S. Li, *Chem. J. Chin. Univ.*, 2003, **24**, 2290.
36. Q. L. Yang, Y. L. Song, M. X. Wan, L. Jiang, W. G. Xu and Q. S. Li, *Chem. J. Chin. Univ.*, 2002, **23**, 1105.
37. S. Meshkova, *J. Fluoresc.*, 2000, **10**, 333.
38. B. Vazquez, S. Deb and W. Bonfield, *J. Mater. Sci.- Mater. Med.*, 1997, **8**, 455.
39. Y. Y. Zheng, X. B. Wang, L. Shang, C. R. Li, C. Cui, W. J. Dong, W. H. Tang and B. Y. Chen, *Mater. Charact.*, 2010, **61**, 489.
40. S. Palaniappan and M. Sairam, *J. Appl. Polym. Sci.*, 2008, **108**, 825.
41. Y. Xia, J. M. Wiesinger, A. G. MacDiarmid and A. J. Epstein, *Chem. Mater.*, 1995, **7**, 443.
42. Q. L. Ma, W. S. Yu, X. T. Dong, J. X. Wang and G. X. Liu, *Nanoscale*, 2014, **6**, 2945.
43. M. O. Ansari, M. M. Khan, S. A. Ansari, J. Lee and M. H. Cho, *RSC Adv.*, 2014, **4**, 23713.